high-resolution computed tomography (HRCT) and the widespread application of CT screening due to the positive results of screening CT trial have enhanced the discovery of small lung cancers, particularly adenocarcinoma (1). These often contain a non-solid component that presents as ground glass opacity (GGO) features on HRCT. Several investigators have reported that GGO is closely associated with bronchioloalveolar carcinoma (BAC) (2).

Recently, the International Association for the Study of Lung Cancer, the American Thoracic Society, and the European Respiratory Society proposed a new classification of lung adenocarcinoma. The terms BAC and mixed subtype adenocarcinoma are no longer used. For resected specimens, new concepts have been introduced such as adenocarcinoma in situ (AIS) and minimally invasive adenocarcinoma (MIA) for small solitary adenocarcinomas with either pure lepidic growth: AIS or predominantly lepidic growth with 5 mm invasion and MIA to define patients who, if they undergo complete resection, will have 100% or near 100% disease-specific survival rates, respectively (3,4). We therefore hypothesized that the GGO component is not related to malignancy or prognosis, implying that only the solid component of the tumor on HRCT (solid tumor size) is indicative of malignancy and prognosis in lung adenocarcinoma.

In this study, we first compared the whole tumor and solid component size, excluding areas of GGO, on preoperative HRCT with a lung window setting and whole tumor size with a mediastinal window setting with pathological whole tumor size and the area of pathologically confirmed invasion. We then determined whether it is more useful to evaluate the whole tumor size or that of only the solid component size to predict the degree of malignancy including lymph node involvement, lymphatic invasion, or vascular invasion of tumors in lung adenocarcinoma.

Material and Methods

Patients

Using preoperative HRCT data of 277 consecutive patients with adenocarcinoma who underwent curative surgical resection from January 2005 to December 2007, we retrospectively measured the whole tumor size and solid component size as follows: the whole tumor and solid component size was measured with lung window setting (WTLW and SCLW) and whole tumor size, with a mediastinal window setting (WTMW) on HRCT. Staging was determined according to the 7th edition of the TNM staging system (5). The histological tumor type was determined according to the World Health Organization (WHO) classification, 3rd edition. In addition, we measured the maximum size of the area pathologically confirmed invasion for this study. We excluded 21 patients with adenocarcinoma with scattered invasive components for this analysis, due to difficulty in measuring not only the pathological invasive area but also the size of the solid component radiologically. Twenty-four patients with inappropriate tissue samples were also excluded following induction therapy or divided tumor resection due to intraoperative frozen diagnosis. Ultimately, 232 consecutive patients with adenocarcinomas were enrolled in this study. Radiological and pathological findings were conducted by SA and JP, and JM and TN, respectively, who were blinded from any clinical information.

Patients were examined at 3-month intervals for the first 2 years and at 6-month intervals for the next 3 years and thereafter on an outpatient basis. The follow-up evaluation involved the following procedures: physical examination, chest radiography, CT of the chest and abdomen, and blood examination, including that of pertinent tumor markers. Further evaluations, including brain magnetic resonance imaging or CT, bone scintigraphy and integrated positron emission tomography, were performed on the first appearance of any symptom or sign of recurrence. The median follow-up time of this series was 4.4 years.

HRCT scanning

Chest images were obtained using 64-detector row CT scanners (LightSpeed VCT: GE Healthcare, Milwaukee, WI, USA and SOMATOM Sensation Cardiac 64: Siemens Medical Systems, Erlangen, Germany) and a 16-detector row CT scanner (BrightSpeed Elite: GE Healthcare, Milwaukee, WI, USA). High-resolution images of the tumors were acquired using the following parameters: 120 kV and auto exposure control; collimation, 0.6–1.25 mm; pitch, 0.9–0.984; 0.4–0.5 s per rotation; reconstructed interval, 1.25–1.5 mm; pixel resolution, 512×512; field of view, 20 cm; and a lung window settings (level = −500/width = 1500 HU) with high spatial frequency algorithm and mediastinal window settings (level = 40/width = 320 HU) with soft-tissue algorithm. GGO was defined as an increase in lung attenuation that did not obscure the underlying vascular markings. We defined the solid tumor size as the maximum dimension of the solid component of the lung windows excluding GGO (SCLW) or the maximum dimension of the whole tumor size of mediastinal setting (WTMW) (Fig. 1a and b).

Pathological findings

Histopathological studies were performed according to WHO criteria, 3rd edition (6). All resected

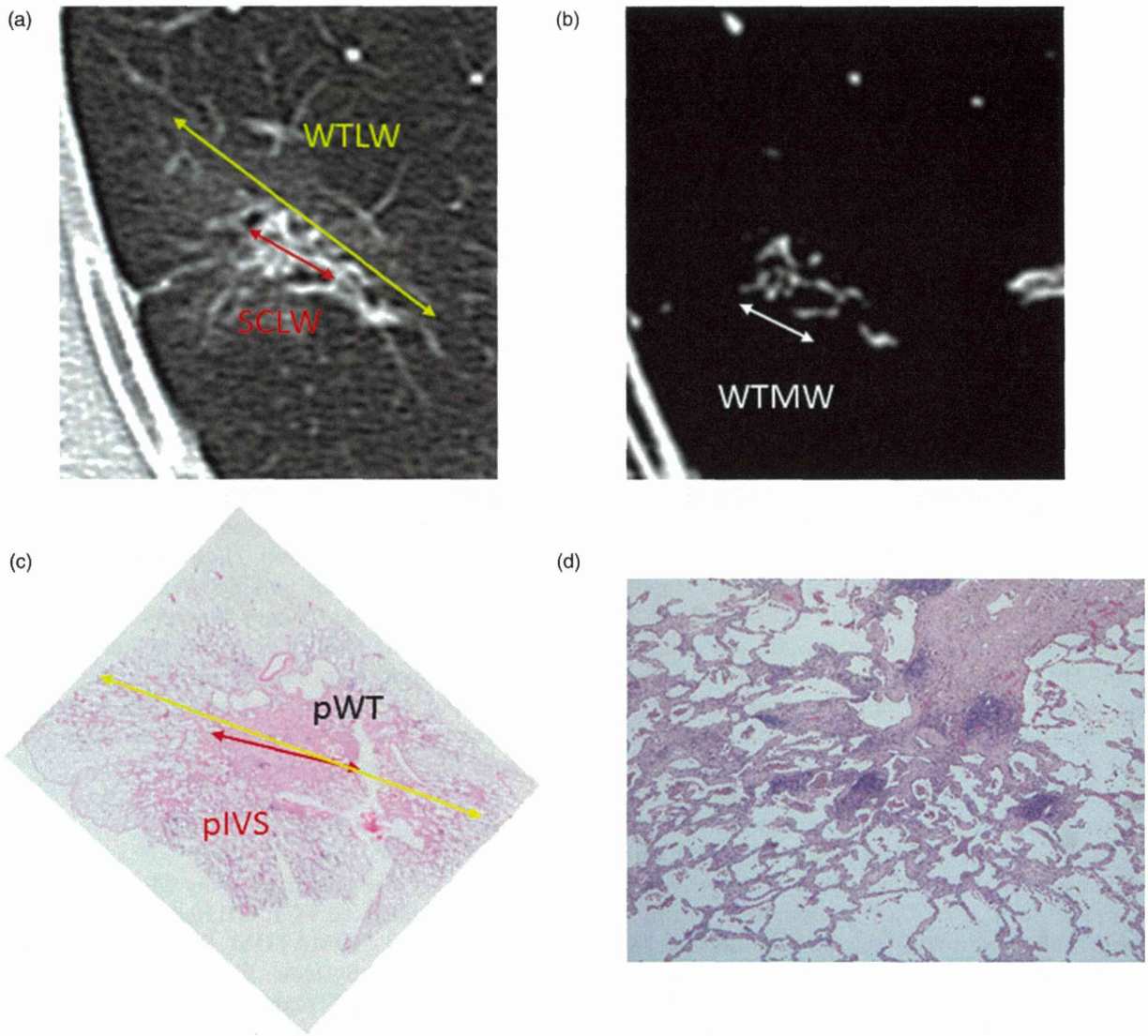

Fig. 1. Correlation between radiological and pathological findings in one typical case. WTLW and SCLW (a), WTMW (b), pWT and pIVS (c), pathological invasive area with high magnification (d). pIVS, pathologically confirmed invasion size; pWT, pathologically confirmed whole tumor size; SCLW, solid component size of lung windows setting; WTLW, whole tumor size of lung windows setting; WTMW, whole tumor size of mediastinal setting.

specimens were formalin-fixed and stained with hematoxylin and eosin in the routine manner. For detailed examinations of lymphatic or vascular invasion or pleural invasion, Elastica van Gieson stain was used to evaluate histological structure and tumor invasion. We also assessed several histological factors: (i) pathological nodal status (pN); (ii) vascular (v) or lymphatic (ly) invasion; and (iii) degree of tumor differentiation (well [G1], moderate [G2], poor [G3]). The maximum size of the pathological whole tumor (pWT) and of the pathological invasive component were measured (pIVS). The maximum size of pWT was assessed by standard gross measurement or histological reconstruction, as necessary. The maximum size of the invasive component was measured microscopically. If the tumor was large, the maximum size of the invasive area was calculated by reconstruction of the tumor slides and measured (Fig. 1c and d). Pathologic high-grade malignancy was defined as lymph node involvement, lymphatic invasion, or vascular invasion.

Statistical analysis

The data are presented as numbers and percentages or mean ± standard deviation, unless otherwise stated. The receiver operating characteristic curves of the whole and solid tumor sizes were used for the

Table 1. Radiological and pathological findings of 232 patients with lung adenocarcinoma.

Variables	*n* (% or range)	
Radiological findings		
WTLW: mean ± SD (cm)	2.59 ± 1.09 (0.73–6.84)	
SCLW: mean ± SD (cm)	2.01 ± 1.18 (0.00–5.78)	
WTMW: mean ± SD (cm)	1.87 ± 1.18 (0.00–5.71)	
Pathological findings		
pT status: pT1a / pT1b / pT2a / pT2b / pT3	86 (37.2) / 68 (29.2) / 61 (26.2) / 6 (2.7) / 11 (4.7)	
pN status: pN0 / pN1 / pN2	195 (83.7) / 20 (8.6) / 17 (7.7)	
pStage: pIA / pIB / pIIA / pIIB / pIIIA	141 (60.5) / 48 (20.6) / 8(3.4) / 8 (3.4) / 27 (12.1)	
pWT: mean ± SD, cm	2.61 ± 1.11 (0.90–7.20)	
pIVS: mean ± SD, cm	2.26 ± 1.27 (0.00–7.2)	
Differentiated: well or poorly	118 (50.6) / 107 (45.9)	ND: 8
Ly: positive / negative	127 (54.5) / 102 (43.8)	ND: 3
V: positive / negative	82 (35.2) / 150 (64.8)	

Ly, lymphatic invasion; ND, no data; pIVS, pathological invasion size; pN, pathological nodal status; pT, pathological T status; pWT, pathological whole tumor size; SCLW, solid component size of lung windows setting; V, vascular invasion; WTLW, whole tumor size of lung windows setting; WTMW, whole tumor size of mediastinal setting.

prediction of lymph node involvement, lymphatic invasion, or vascular invasion or well differentiation. We also performed multiple logistic regression analysis to determine the independent variables related to the whole tumor size and the solid tumor size for the prediction of the pathologic finding of high-grade malignancy. Overall survival (OS) was calculated from the date of surgery to the time of death. Observations were censored at final follow-up if the patient was living. Disease-free survival (DFS) was defined as the interval from the date of surgery until the first event (relapse or death from any cause) or the last follow-up visit. The duration of DFS was analyzed using the Kaplan-Meier method. Differences in OS or DFS were assessed using the log-rank test. To assess the potential independent and valuable prognostic effects of clinical tumor size on OS or DFS, we performed multivariate analysis with the Cox proportional hazards model using variables with $P < 0.05$. The data were statistically analyzed using the Statistical Package for Social Sciences software, version 10.5 (SPSS Inc., Chicago, IL, USA).

Ethical considerations

The approval of the Institutional Review Board of Tokyo Medical University was obtained (project approval No. 1665), but as this was a retrospective study the need to obtain written informed consent from either the patients or their representatives was waived, in accordance with the American Medical Association Manual of Style (10th edition).

Results

Patient characteristics

There were 118 (51.0%) women and 114 (49.0%) men aged 35–86 years (mean, 65.0 years). The several radiological and pathological findings of 232 patients are summarized in Table 1.

Correlation between radiological and pathological findings

Fig. 2 shows several correlations between radiological findings including WTLW, SCLW, or WTMW, and pathological findings including pWT or pIVS. There were significant correlations between SCLW and pIVS ($R = 0.762$, 95% CI = 0.702–0.811, $P < 0.0001$), WTMW and pIVS ($R = 0.771$, 95% CI = 0.713–0.819, $P < 0.0001$), and WTLW and pIVS ($R = 0.792$, 95% CI = 0.735–0.835, $P < 0.0001$), respectively.

Receiver operating characteristic curve

The receiver operating characteristic area under the curve values of WTLW, SCLW, WTMW, and pIVS used for predicting lymph node involvement, lymphatic invasion, vascular invasion, degree of differentiation, and pathologic high-grade malignancy (lymph node involvement or lymphatic or vascular invasion) are given in Table 2 and Fig. 3. The predictability of all outcomes on the basis of solid tumor size such as SCLW and WTMW was better than that using the

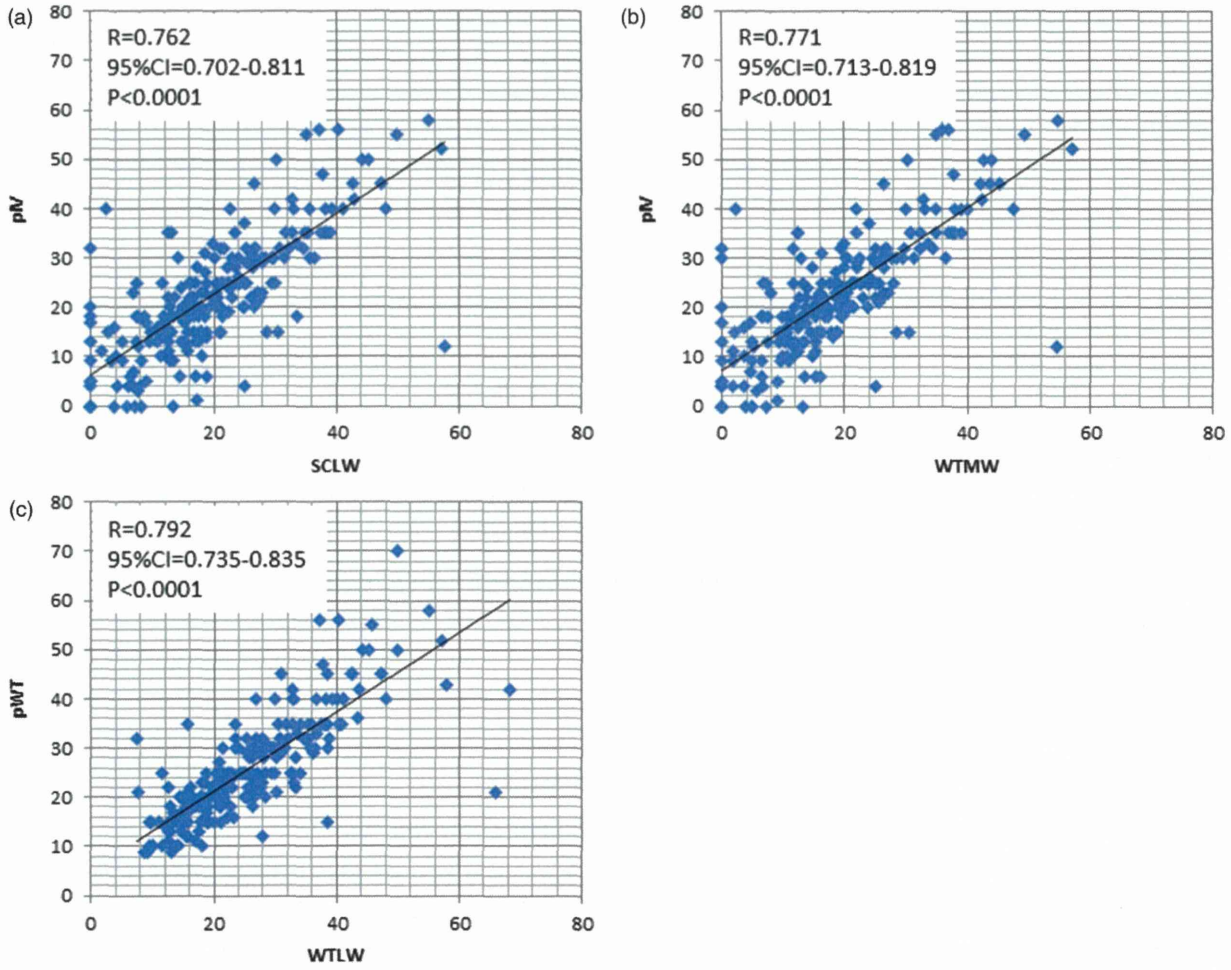

Fig. 2. Correlative graphs between radiological and pathological findings. There were significant correlations between SCLW and pIVS (R = 0.762, 95% CI = 0.702–0.811, $P < 0.0001$) (a), WTMW and pIVS (R = 0.771, 95% CI = 0.713–0.819, $P < 0.0001$) (b), and WTLW and pIVS (R = 0.792, 95% CI = 0.735–0.835, $P < 0.0001$) (c), respectively. pIVS, pathologically confirmed invasion size; pWT, pathologically confirmed whole tumor size; SCLW, solid component size of lung windows setting; WTLW, whole tumor size of lung windows setting; WTMW, whole tumor size of mediastinal setting.

Table 2. Receiver operative characteristic area under the curve values of WTLW, SCLW, WTMW, and pIVS used to predict pathologic findings.

	WTLW		SCLW		WTMW		pIVS	
Variable	AUC (95% CI)	*P* value	AUC (95% CI)	*P* value	AUC (95% CI)	*P* value	AUC (95% CI)	*P* value
pN	0.711 (0.625–0.797)	<0.0001	0.796 (0.723–0.870)	<0.0001	0.809 (0.737–0.880)	<0.0001	0.788 (0.717–0.859)	<0.0001
Ly	0.685 (0.616–0.754)	<0.0001	0.793 (0.735–0.852)	<0.0001	0.801 (0.744–0.859)	<0.0001	0.772 (0.711–0.833)	<0.0001
V	0.646 (0.593–0.719)	<0.0001	0.766 (0.704–0.828)	<0.0001	0.769 (0.706–0.831)	<0.0001	0.777 (0.717–0.837)	<0.0001
pN or Ly or V	0.693 (0.623–0.762)	<0.0001	0.817 (0.761–0.873)	<0.0001	0.824 (0.769–0.879)	<0.0001	0.796 (0.733–0.855)	<0.0001
Well diff.	0.623 (0.551–0.695)	0.001	0.770 (0.710–0.830)	<0.0001	0.771 (0.711–0.832)	<0.0001	0.770 (0.709–0.830)	<0.0001

Ly, lymphatic invasion; pIVS, pathological invasion size; pN, pathological lymph node status; SCLW, solid component size of lung windows setting; V, vascular invasion; Well diff., well differentiated; WTLW, whole tumor size of lung windows setting; WTMW, whole tumor size of mediastinal setting.

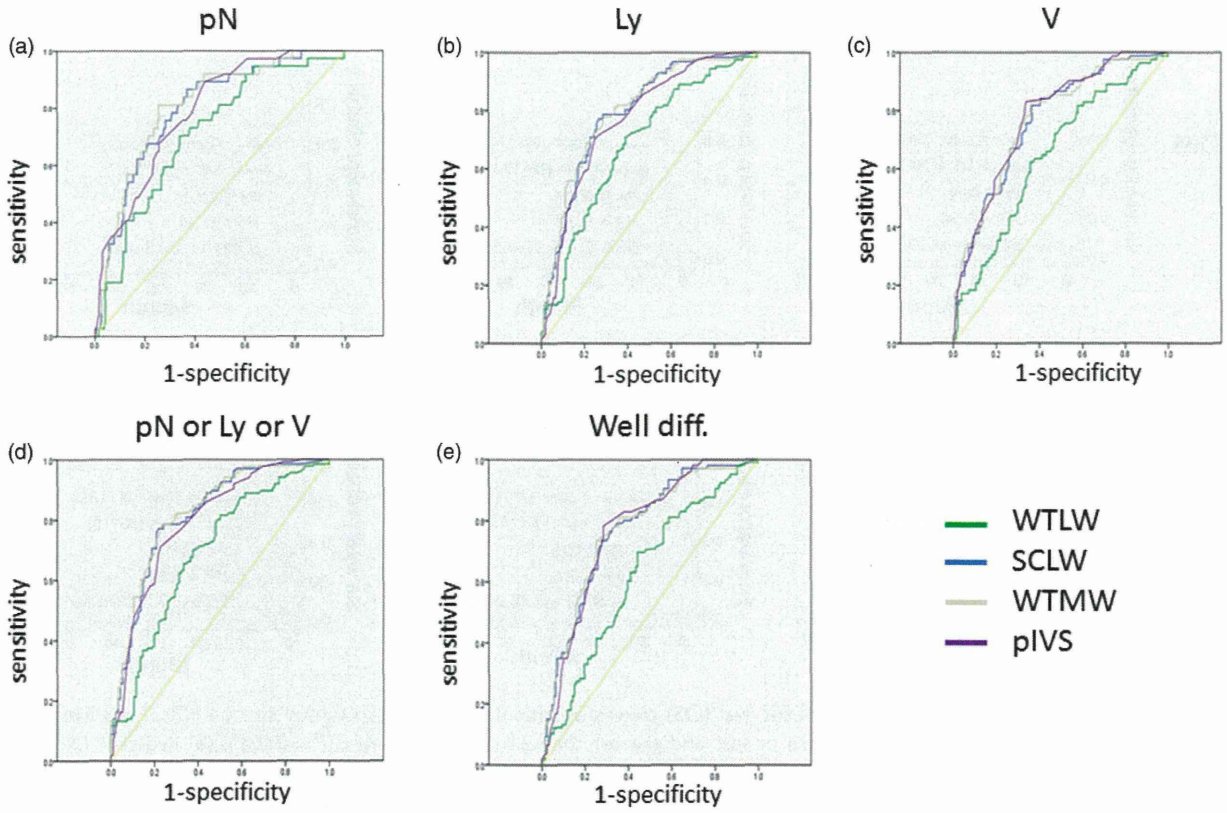

Fig. 3. Receiver operating characteristic area under the curve for detecting (a) pathological lymph node metastasis (pN), (b) lymphatic invasion (Ly), (c) vascular invasion (V), (d) high-grade malignancy (pN, VI, or PI), and (e) degree of differentiation for radiological whole and solid tumor sizes including WTLW, SCLW, and WTMW and pathological invasion area, pIVS. SCLW, solid component size of lung windows setting; WTLW, whole tumor size of lung windows setting; WTMW, whole tumor size of mediastinal setting.

whole tumor size that is WTLW for all subjects. The receiver operating characteristic curves of SCLW and WTMW were similar to that of pIVS that is pathological confirmed invasion area.

Survival significance

We assessed survival significance of preoperative radiological findings including WTLW, SCLW, and WTMW. Patients were categorized into radiological measurement of tumor size greater than 2 cm or those 2 cm or less according to WTLW, SCLW, and WTMW. There were significant differences in both the DFS and OS of this series according to SCLW ($P = 0.0001$ and $P = 0.023$) and WTMW ($P < 0.0001$ and $P = 0.008$), respectively (Fig. 4). Moreover, to find the most valuable and independent radiological prognostic factor including WTLW, SCLW, and WTMW as a candidate of next T factor, we performed multivariate analysis of DFS and OS. Table 3 revealed that WTMW (HR = 0.72, 95% CI = 0.58–0.90, $P = 0.004$ and HR = 0.74, 95% CI = 0.57–0.96, $P = 0.022$, respectively) was the independent prognostic factor among preoperative variables among age, sex, WTLW, and SCLW in this series.

Discussion

The frequency of identification of small lung cancers has increased since CT and enhanced scanning have become routine procedures. Small tumors, especially in lung adenocarcinomas, often contain GGO components as visualized on HRCT (2,7–9). Noguchi et al. first reported that type A and B small peripheral adenocarcinomas (localized bronchioloalveolar carcinoma without foci of active fibroblastic proliferation) showed no lymph node metastasis and a favorable prognosis (100% 5-year survival rate) (10). In 2011, new concepts were introduced including AIS and MIA. Because some of these cancers did not show growth for a long period, controversy remains as to how to manage subsolid nodules (11–14). Furthermore, both subsolid nodules and AIS have been discussed in relation to over diagnosis, which is defined as a diagnosis of lung cancer that would not lead to an individual's death because of the slow

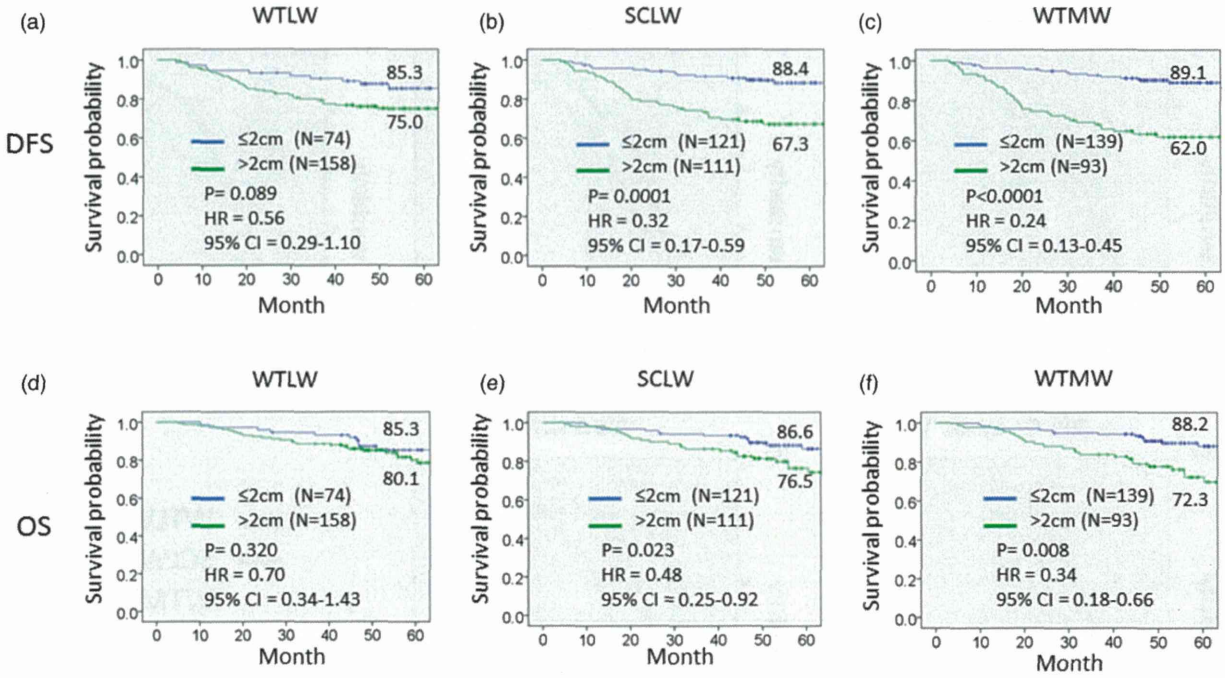

Fig. 4. Disease-free survival (DFS) and overall survival (OS) curves of patients according to tumor size on HRCT. (a) five-year DFS rate of 85.3% and 75.0% for a WTLW of 2.0 cm or less and greater than 2.0 cm, respectively ($P = 0.089$). (b) five-year DFS rate of 88.4% and 67.3% for a SCLW of 2.0 cm or less and greater than 2.0 cm, respectively ($P = 0.0001$). (c) five-year DFS rate of 89.1% and 62.0% for a WTMW of 2.0 cm or less and greater than 2.0 cm, respectively ($P < 0.0001$). (d) five-year OS rate of 85.2% and 80.1% for a WTLW of 2.0 cm or less and greater than 2.0 cm, respectively ($P = 0.320$). (e) five-year OS rate of 86.6% and 76.5% for a SCLW of 2.0 cm or less and greater than 2.0 cm, respectively ($P = 0.023$). (f) five-year OS rate of 88.2% and 72.3% for a WTLW of 2.0 cm or less and greater than 2.0 cm, respectively ($P = 0.008$). SCLW, solid component size of lung windows setting; WTLW, whole tumor size of lung windows setting; WTMW, whole tumor size of mediastinal setting.

Table 3. Multivariate analysis of DFS and OS.

		DFS			OS		
Variable	Category	HR	95% CI	*P* value	HR	95% CI	*P* value
Age (years)	<70						
	≥70	1.57	0.82–3.01	0.177	1.14	0.57–2.26	0.715
Sex	Men						
	Women	0.97	0.54–1.74	0.911	0.603	0.30–1.20	0.148
WTLW		0.94	0.89–1.00	0.040*	0.97	0.92–1.03	0.345
SCLW		0.82	0.66–1.01	0.067	0.80	0.62–1.03	0.078
WTMW		0.72	0.58–0.90	0.004 *	0.74	0.57–0.96	0.022*

*Statistically significant.

CI, confidence interval; DFS, disease-free survival; HR, hazard ratio; OS, overall survival; SCLW, solid component size of lung windows setting; WTLW, whole tumor size of lung windows setting; WTMW, whole tumor size of mediastinal setting.

growth rate and competing age-related risks for death (15–18).

The general concept of TNM classification by UICC is that "For consistency, in the TNM system, carcinoma in situ is categorized as Stage 0", according to the 7^{th} edition of the TNM Classification of Malignant Tumours (19), which means AIS itself should not be used for staging grouping. However, clinical physicians specializing in lung cancer measure the tumor size by including the GGO components visualized on HRCT. On the basis of our hypothesis that the solid components, not the GGO components, of tumors as

visualized on HRCT, indicate malignancy and prognosis, we evaluated the role of solid tumor size (the size without the GGO component) in cases of lung adenocarcinoma.

First, we demonstrated that correlations between radiological findings including WTLW, SCLW, or WTMW, and pathological findings including pWT or pIVS. There were significant correlations between pIVS and SCLW or WTMW and between pWT and WTLW. Next we analyzed sensitivity and specificity of these radiological factors for predicting pathological malignant factors including lymph node involvement, lymphatic invasion, vascular invasion, and differentiation of the tumor. All receiver operating characteristic areas under the curves for predicting pN, Ly, V, high-grade malignancy (pN or Ly or V) and well differentiation were greater in the solid components size which is SCLW and WTMW than those for the whole tumor size which is WTLW. Because the range of mean radiological measurement of WTLW, SCLW and WTMW were from 1.87 to 2.59 cm in size and the cutoff point of 2 cm is also used as T factor. Finally, we analyzed each DFS and OS according to the cutoff point of 2 cm using whole and solid tumor sizes. Kaplan-Meier curves of both DFS and OS showed better division according to the solid components size, SCLW and WTMW, compared with the whole tumor size, WTLW. Moreover, multivariate analysis revealed that WTMW were identified as independent predictive factors for both DFS and OS. These results indicate that solid tumor size, not whole tumor size, more closely reflects the pathologic findings and those related to clinical tumor malignancy.

Several investigators have reported that the prognosis of patients with lung adenocarcinoma and a large GGO component visualized on HRCT was much better than that of patients with other adenocarcinoma types, irrespective of the maximal tumor dimension (20–23). In addition, JCOG0201, a multicenter prospective radiological study has examined the specificity, sensitivity, and accuracy of the radiologic diagnoses of lymphatic/vessel invasion and nodal involvement of clinical T1N0M0 adenocarcinoma made according to the HRCT findings (24). Recently, a multicenter registration study demonstrated that solid tumor size on HRCT and maximum standardized uptake values on PET/CT has greater predictive value for high-grade malignancy and prognosis in clinical stage IA lung adenocarcinoma than that of whole tumor size (25). This final result indicated that using the solid tumor size is much simpler than using the GGO ratio; furthermore, the solid tumor size can be applied to the T descriptor in the TNM classification.

In this study, patients with lung adenocarcinoma were eligible for assessment and approximately one-third of the patients with whole tumors greater than 3 cm were included in final analysis. This confirmation of the significance of using the solid component for prognosis is consistent with previous studies using small-sized lung adenocarcinoma. Therefore, this result suggested that this concept of using solid tumor size can be applied to the T descriptor of TNM classification for larger tumors.

To the best of our knowledge, this is the first study demonstrating the correlation between radiological and pathological findings and the prognostic significance of solid tumor size in lung adenocarcinoma including tumors larger than 3 cm. However, there are several limitations in this study. First, this was a medium-size retrospective, single-institution analysis. Second, to clarify and simplify measuring the radiological and pathological size, we excluded lung adenocarcinoma with scattered invasive components which were slightly less than 10% of the population. It remains unclear whether we should count the largest scattered invasive components or the sum total of them. Third, we used two radiological measurements, SCLW and WTMW, in this analysis. Our results suggested that using WTMW counting for solid invasive components might be a better mediator for prognostic outcome of lung adenocarcinoma compared with SCLW, which is consistent with some of the previous. It remains unclear whether WTMW or SCLW should be a better predictor. Therefore, larger and multicenter studies using identical protocols are needed.

In conclusion, the predictive values of solid tumor size visualized on HRCT especially in mediastinal windows for pathologic high-grade malignancy and prognosis in patients with lung adenocarcinoma were greater than those of the whole tumor size. We recommend that the solid tumor size be used to determine the T descriptor in the TNM classification of lung tumor and be defined as the true tumor size in cases of lung adenocarcinoma with a GGO component visualized on HRCT.

Acknowledgements

We are indebted to Professor James M. Vardaman of Waseda University and Professor J Patrick Barron, Chairman of the Department of International Medical Communications of Tokyo Medical University, for their editorial review of the English manuscript.

Conflict of interest

None declared.

Funding

This study was supported by a Grant-in-Aid for Scientific Research, Japan Society for the Promotion of Science (24592104), Ministry of Education, Culture, Sports, Science and Technology, Japan.

References

1. Aberle DR, Adams AM, Berg CD, et al. Reduced lung-cancer mortality with low-dose computed tomographic screening. N Engl J Med 2011;365:395–409.
2. Nakata M, Saeki H, Takata I, et al. Focal ground-glass opacity detected by low-dose helical CT. Chest 2002;121: 1464–1467.
3. Travis WD, Brambilla E, Noguchi M, et al. International Association for the Study of Lung Cancer/American Thoracic Society/European Respiratory Society: international multidisciplinary classification of lung adenocarcinoma: executive summary Proc Am Thorac Soc 2011;8:381–385.
4. Lee HJ, Goo JM, Lee CH, et al. Predictive CT findings of malignancy in ground-glass nodules on thin-section chest CT: the effects on radiologist performance. Eur Radiol 2009;19:552–560.
5. Goldstraw P, Crowley J, Chansky K, et al. The IASLC Lung Cancer Staging Project: proposals for the revision of the TNM stage groupings in the forthcoming (seventh) edition of the TNM Classification of malignant tumours. J Thorac Oncol 2007;2:706–714.
6. Travis WD, Brambilla E, Muller-Hermelink H, et al. World Health Organization Classification of Tumours: Pathology & Genetics Tumours of the Lung, Pleura, Thymus and Heart, 3rd edn. Lyon: IARC Press, 2004.
7. Okada M, Koike T, Higashiyama M, et al. Radical sublobar resection for small-sized non-small cell lung cancer: a multicenter study. J Thorac Cardiovasc Surg 2006;132: 769–775.
8. Nakayama H, Yamada K, Saito H, et al. Sublobar resection for patients with peripheral small adenocarcinomas of the lung: surgical outcome is associated with features on computed tomographic imaging. Ann Thorac Surg 2007;84:1675–1679.
9. Suzuki K, Kusumoto M, Watanabe S, et al. Radiologic classification of small adenocarcinoma of the lung: radiologic-pathologic correlation and its prognostic impact. Ann Thorac Surg 2006;81:413–419.
10. Noguchi M, Morikawa A, Kawasaki M, et al. Small adenocarcinoma of the lung. Histologic characteristics and prognosis. Cancer 1995;75:2844–2852.
11. Kodama K, Higashiyama M, Yokouchi H, et al. Natural history of pure ground-glass opacity after long-term follow-up of more than 2 years. Ann Thorac Surg 2002; 73:386–92; discussion 92–93.
12. Takashima S, Maruyama Y, Hasegawa M, et al. CT findings and progression of small peripheral lung neoplasms having a replacement growth pattern. Am J Roentgenol 2003;180:817–826.
13. Hiramatsu M, Inagaki T, Matsui Y, et al. Pulmonary ground-glass opacity (GGO) lesions-large size and a history of lung cancer are risk factors for growth. J Thorac Oncol 2008;3:1245–1250.
14. Sawada S, Komori E, Nogami N, et al. Evaluation of lesions corresponding to ground-glass opacities that were resected after computed tomography follow-up examination. Lung Cancer 2009;65:176–179.
15. Henschke CI, Yankelevitz DF, Mirtcheva R, et al. CT screening for lung cancer: frequency and significance of part-solid and nonsolid nodules. Am J Roentgenol 2002; 178:1053–1057.
16. Toyoda Y, Nakayama T, Kusunoki Y, et al. Sensitivity and specificity of lung cancer screening using chest low-dose computed tomography. Br J Cancer 2008;98: 1602–1607.
17. Jett JR. Limitations of screening for lung cancer with low-dose spiral computed tomography. Clin Cancer Res 2005;11:4988s–4992s.
18. Goo JM, Park CM, Lee HJ. Ground-glass nodules on chest CT as imaging biomarkers in the management of lung adenocarcinoma. Am J Roentgenol 2011;196: 533–543.
19. Sobin LH, Gospodarowicz MK, Wittekind C. TNM Classification of Malignant Tumours. Oxford: John Wiley & Sons, Ltd., 2009.
20. Aoki T, Tomoda Y, Watanabe H, et al. Peripheral lung adenocarcinoma: correlation of thin-section CT findings with histologic prognostic factors and survival. Radiology 2001;220:803–809.
21. Suzuki K, Asamura H, Kusumoto M, et al. "Early" peripheral lung cancer: prognostic significance of ground glass opacity on thin-section computed tomographic scan. Ann Thorac Surg 2002;74:1635–1639.
22. Ohde Y, Nagai K, Yoshida J, et al. The proportion of consolidation to ground-glass opacity on high resolution CT is a good predictor for distinguishing the population of non-invasive peripheral adenocarcinoma. Lung Cancer 2003;42:303–310.
23. Tsutani Y, Miyata Y, Yamanaka T, et al. Solid tumors versus mixed tumors with a ground-glass opacity component in patients with clinical stage IA lung adenocarcinoma: Prognostic comparison using high-resolution computed tomography findings. J Thorac Cardiovasc Surg 2013;146:17–23.
24. Suzuki K, Koike T, Asakawa T, et al. A prospective radiological study of thin-section computed tomography to predict pathological noninvasiveness in peripheral clinical IA lung cancer (Japan Clinical Oncology Group 0201). J Thorac Oncol 2011;6:751–756.
25. Tsutani Y, Miyata Y, Nakayama H, et al. Prognostic significance of using solid versus whole tumor size on high-resolution computed tomography for predicting pathologic malignant grade of tumors in clinical stage IA lung adenocarcinoma: a multicenter study. J Thorac Cardiovasc Surg 2012;143:607–612.

European Journal of Cardio-Thoracic Surgery 46 (2014) e120–e126
doi:10.1093/ejcts/ezu375 Advance Access publication 23 October 2014

ORIGINAL ARTICLE

High-quality 3-dimensional image simulation for pulmonary lobectomy and segmentectomy: results of preoperative assessment of pulmonary vessels and short-term surgical outcomes in consecutive patients undergoing video-assisted thoracic surgery†

Masaru Hagiwara[a], Yoshihisa Shimada[a,*], Yasufumi Kato[a], Kimitoshi Nawa[a], Yojiro Makino[a], Hideyuki Furumoto[a], Soichi Akata[b], Masatoshi Kakihana[a], Naohiro Kajiwara[a], Tatsuo Ohira[a], Hisashi Saji[c] and Norihiko Ikeda[a]

[a] First Department of Surgery, Tokyo Medical University Hospital, Tokyo, Japan
[b] Department of Radiology, Tokyo Medical University Hospital, Tokyo, Japan
[c] Department of Chest Surgery, St. Marianna University School of Medicine, Yokohama, Japan

* Corresponding author. First Department of Surgery, Tokyo Medical University Hospital, 6-7-1 Nishishinjuku, Shinjuku-ku, Tokyo 160-0023, Japan. Tel: +81-3-33426111; fax: +81-3-33426203; e-mail: zenkyu@za3.so-net.ne.jp (Y. Shimada).

Received 16 May 2014; received in revised form 24 July 2014; accepted 1 August 2014

Abstract

OBJECTIVES: The aim of this study was to evaluate the effectiveness of 3-dimensional computed tomography (3D-CT) software in short-term surgical outcomes and the assessment of variations of pulmonary vessel branching patterns on performing video-assisted thoracic surgery (VATS).

METHODS: The study included 179 consecutive patients who had undergone VATS anatomical lung resection, of which 172 were lobectomies (96%) and 7 were segmentectomies (4%), from May 2011 through January 2013. There were 124 patients (69%) in whom 3D-CT was performed and 55 patients (31%) who had not undergone 3D-CT. Observed actual pulmonary vessel branching patterns by intraoperative findings or footage were compared with the 3D image findings. Various surgical outcomes, including the occurrence of postoperative complications, in this study defined as those of Grade 2 or above under the Clavien–Dindo classification system, and total operative time, were retrieved from available clinical records.

RESULTS: Among the 124 patients with preoperative 3D imaging, there were 5 (4%) conversions from VATS to thoracotomy. The incidence rate of patients with postoperative complications was 8% ($n = 10$), and there were no 30-day or 90-day mortalities. Pulmonary artery (PA) branches were precisely identified for 97.8% (309 of 316) of branches on 3D images, and the sizes of the seven undetected branches (five in the right upper lobe, two in the left upper lobe) ranged from 1 to 2 mm. The 3D images accurately revealed 15 cases (12%) of anomalous or unusual PA branches and 5 cases (4%) of variant pulmonary veins. Multivariate logistic regression analysis of the association with postoperative complications and operative time in 165 lung cancer patients demonstrated that male gender was the only statistically significant independent predictor of complications (risk ratio: 5.432, $P = 0.013$), and patients without 3D imaging tended to have operative complications (risk ratio: 2.852, $P = 0.074$), whereas conducting the 3D-CT (risk ratio: 2.282, $P = 0.021$) as well as intraoperative bleeding amount (risk ratio: 1.005, $P = 0.005$) had significant association with operative time.

CONCLUSIONS: High-quality 3D-CT images clearly revealed the anatomies of pulmonary vessels, which could play important roles in safe and efficient VATS anatomical resection.

Keywords: 3-Dimensional computed tomography • Simulation • Video-assisted thoracic surgery • Lobectomy • Pulmonary vessels

INTRODUCTION

Video-assisted thoracic surgery (VATS) lobectomy and segmentectomy have been established as standard surgical techniques for the treatment of lung cancer, metastatic lung tumours and benign lung tumours. A number of reports have documented the safety and effectiveness of a thoracoscopic approach, which has less morbidity, better postoperative respiratory function and equivalent oncological outcomes to conventional thoracotomy [1–4]. Anatomical variants of pulmonary vessels can cause serious problems such as unexpected bleeding in patients undergoing VATS [5, 6]. Detailed preoperative understanding and simulations of the surgical anatomy using image modalities would greatly contribute to safely performing VATS.

†Presented at the 22nd European Conference on General Thoracic Surgery, Copenhagen, Denmark, 15–18 June 2014.

Multidetector computed tomography (MDCT) allows surgeons to construct 3-dimensional (3D) images of lung structures. We have used 3D lung modelling based on CT images taken using the Fujifilm Synapse Vincent system (Fujifilm Corporation, Tokyo, Japan) to obtain 3D images of the pulmonary vessels and the tracheobronchial tree for surgical simulations [7, 8]. Several reports have addressed the usefulness of pre- or intraoperative use of 3D evaluations in the field of thoracic surgery [7–12]. However, the influence of 3D simulation on perioperative surgical outcomes in VATS has not been well described. The aim of this study was to evaluate the effectiveness of 3D software in short-term surgical outcomes and the preoperative assessment of variations of pulmonary vessel branching patterns for safely performing VATS.

PATIENTS AND METHODS

Patients

From May 2011 to January 2013, 561 patients underwent pulmonary resection at our department. Among them, 179 (31.9%) consecutive patients who had undergone VATS anatomical lung resections were included in this retrospective study. Our original indications of VATS anatomical resection for malignancies were for peripheral tumours less than 5 cm in diameter without nodal involvement. However, we have applied the VATS procedure in patients with multiple comorbidities who would otherwise not be suitable candidates for the conventional thoracotomy approach. We have preoperatively constructed 3D lung modelling based on CT images of lung structures taken using the Synapse Vincent system for the majority of patients scheduled for VATS lobectomy or segmentectomy. Data collection and analyses were approved and the need to obtain written informed consent from each patient was waived by the Institutional Review Board of Tokyo Medical University.

Preoperative 3D image construction and simulation

Patients underwent CT imaging with a 64-channel MDCT (Light Speed VCT, GE Medical Systems, Milwaukee, WI, USA) set at the following parameters: gantry rotation speed of 0.4 s per rotation, collimation of 0.625 mm, table incrementation speed of 39.37 mm/s with a helical pitch of 0.984, tube voltage of 120 kV, and the tube current was used with an automatic exposure control system. Axial sections (1.25 mm in thickness) were reconstructed at intervals of 1.0 mm. A total of 100 ml of iohexol (Omnipaque, 300 mg of iodine per ml; Daiichi-Sankyo Pharmaceutical, Tokyo, Japan) was injected by a mechanical injector (Dual Shot GX7; Nemoto Kyorindo, Tokyo, Japan) at a rate of 1.5–2.0 ml/s without an injection of saline solution afterwards. Each CT image was acquired within 1 breath hold of about 5 s, after a delay of 70 s during which the contrast media injection took effect. The presented CT scan protocol has been used for not only the 3D image construction but also standard staging for lung cancer patients to be suitable for contrast radiography. These digital imaging and communication in medicine data were transferred to a workstation with the volume-rendering reconstruction software. After this step, a surgeon can construct 3D images completed within approximately 5 min for surgical simulations. We have performed VATS with double monitor guidance: one was a thoracoscopy television monitor, and the other was the 3D imaging system. The simulation system was implemented as a plug-in in the processing workstation (Dell Precision T5500, Windows 7 Professional, 64-bit, 12 GB, DDR3 RDIMM).

Operative procedure

Operations were performed with the patient in the lateral decubitus position under general anaesthesia with one-lung ventilation. Three or four incisions were used in each patient. A 10-mm camera port was placed in the sixth intercostal space (ICS) at the midaxillary line, through which a 30-degree thoracoscope was positioned. An access incision of 3 cm was placed in the fourth ICS and centred at the anterior axillary line, and a 10-mm accessory port was placed in the sixth ICS at the anterior axillary line. A 15-mm assist port was placed at the tip of the scapula. Rib resection or rib spreading was not performed.

Analysing evaluation data

To determine the ability of 3D images to enable the assessment of pulmonary artery (PA) branching patterns involved in operation, vascular size, the route of the pulmonary vein (PV) and the results of all examinations were interpreted by two surgeons (at least one of whom was a board-certified thoracic surgeon) and one chest radiologist (Soichi Akata) in consensus. The intraoperative footage was postoperatively evaluated by two surgeons, who were blinded to patient identification. When pulmonary vessels identified by the footage could not be visualized in the 3D images, they were considered 'undetected' vessel branches. Short-term outcomes, such as operating time, approximate blood loss, mortality rate and postoperative complications, were retrieved from available clinical records. The development of postoperative complications in this study was defined as Grade 2 or above for severe complications under the Clavien–Dindo classification system.

Statistical analysis

The χ^2 test and Fisher's exact or Student's *t*-test were used to compare proportions and continuous variables in analysing the frequency of occurrence of postoperative complications and operative time. Multivariate analyses were performed using the multiple logistic regression analysis, and we checked the validity of the model using the Hosmer–Lemeshow χ^2 test (a larger *P* value signifies greater reliability) on an external validation data set. All tests were two-sided, and *P*-values less than 0.05 were considered to indicate a statistically significant difference between the two groups. All statistical calculations were performed using the SPSS statistical software package (version 21.0; DDR3 RDIMM, SPSS, Inc., Chicago, IL, USA).

RESULTS

The characteristics of the patients who underwent VATS anatomical lung resection during this study period are summarized in Table 1. The study cohort of 179 patients included 88 men and 91 women, of whom 165 (92%) had primary lung cancer and 172